Drogue-Loss Detection for Surface Drifters during the Lagrangian Submesoscale Experiment (LASER)

A. C. HAZA,[a] E. D'ASARO,[b] H. CHANG,[c] S. CHEN,[d] M. CURCIC,[d] C. GUIGAND,[a] H. S. HUNTLEY,[c] G. JACOBS,[e] G. NOVELLI,[a] T. M. ÖZGÖKMEN,[a] A. C. POJE,[f] E. RYAN,[a] AND A. SHCHERBINA[b]

[a] *Rosenstiel School of Marine and Atmospheric Science, University of Miami, Miami, Florida*
[b] *Applied Physics Laboratory, and School of Oceanography, University of Washington, Seattle, Washington*
[c] *School of Marine Science and Policy, University of Delaware, Newark, Delaware*
[d] *Department of Atmospheric Sciences, University of Washington, Seattle, Washington*
[e] *Naval Research Laboratory, Stennis Space Center, Mississippi*
[f] *Department of Mathematics, City College of the City University of New York, New York, New York*

(Manuscript received 24 August 2017, in final form 17 January 2018)

ABSTRACT

The Lagrangian Submesoscale Experiment (LASER) was designed to study surface flows during winter conditions in the northern Gulf of Mexico. More than 1000 mostly biodegradable drifters were launched. The drifters consisted of a surface floater extending 5 cm below the surface, containing the satellite tracking system, and a drogue extending 60 cm below the surface, hanging beneath the floater on a flexible tether. On some floats, the drogue separated from the floater during storms. This paper describes methods to detect drogue loss based on two properties that distinguish drogued from undrogued drifters. First, undrogued drifters often flip over, pointing their satellite antenna downward and thus intermittently reducing the frequency of GPS fixes. Second, undrogued drifters respond to wind forcing more than drogued drifters. A multistage analysis is used: first, two properties are used to create a preliminary drifter classification; then, the motion of each unclassified drifter is compared to that of its classified neighbors in an iterative process for nearly all of the drifters. The algorithm classified drifters with a known drogue status with an accuracy of virtually 100%. Drogue loss times were estimated with a precision of less than 0.5 and 3 h for 60% and 85% of the drifters, respectively. An estimated 40% of the drifters lost their drogues in the first 7 weeks, with drogue loss coinciding with storm events, particularly those with steep waves. Once the drogued and undrogued drifters are classified, they can be used to quantify the differences in material dispersion at different depths.

1. Introduction

The Lagrangian Submesoscale Experiment (LASER) was designed to study near-surface physical processes during winter conditions in the northern Gulf of Mexico (NGoM) as part of the long-term objective of understanding oil dispersion. The study was motivated by the Deepwater Horizon oil spill in 2010, the largest accidental marine oil spill in history. Observations of oil spills show complex patterns—most notably accumulation and transport in small-scale convergence zones—that are not predicted by traditional transport models that assume nondivergent flows (Zhong et al. 2012; Huntley et al. 2015; Haza et al. 2016). Recent progress in the understanding of submesoscale flows (McWilliams 2016) provides a new theoretical basis for these surface convergence regions. To test some of these theories in the field, high-resolution Lagrangian measurements of surface flow are needed, with a large number of drifters capturing scales from tens of kilometers to tens of meters, to resolve both larger-scale nondivergent and smaller-scale divergent features. Toward this goal, the new Consortium for Advanced Research on Transport of Hydrocarbon in the Environment (CARTHE) surface drifter was designed (Novelli et al. 2017; Lumpkin et al. 2017). The environmentally friendly design used injection-molded biodegradable plastic components that could be inexpensively produced, easily assembled, and hand deployed (Fig. 1a). The drifter was extensively tested to minimize wave rectification and wind slip and to verify that this design accurately tracked the average horizontal current in the upper 60 cm. More than 1000 units were deployed during LASER in January

Corresponding author: Angelique Haza, ahaza@rsmas.miami.edu

DOI: 10.1175/JTECH-D-17-0143.1

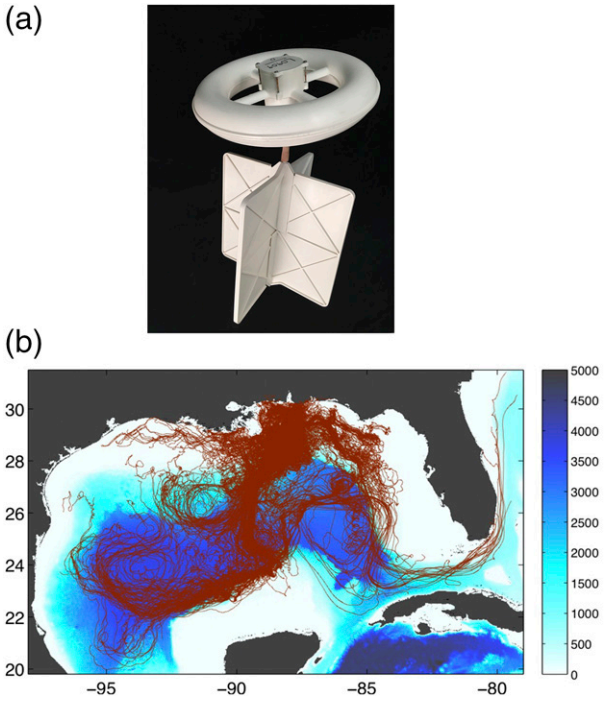

FIG. 1. (a) The CARTHE drifter, composed of a biodegradable donut-shaped floater, housing a GPS and batteries, and a drogue made of four biodegradable sails, connected by a flexible rubber tube. (b) The LASER drifter trajectories, superimposed onto the GoM topography (depth; m).

through February 2016 in the DeSoto Canyon region of the NGoM.

More than 1000 drifters were released during this experiment. The experiment was in part composed of three large deployments of about 300 drifters each, including two in tightly packed configurations on the continental slope of the NGoM.

Unusually strong storms occurred during LASER as the result of the 2016 El Niño, with the most intense episodes occurring 22 and 27 January; 5, 9, 15, and 24 February; and 9 March. In particular, major storms occurred 1–2 days after the dense drifter launches of 21 January and 7 February. Substantial fractions of the drifters lost their drogues during these events, resulting in a mixture of drogued and undrogued drifters within a small area. The two different groups rapidly developed distinct drift patterns. Accurate estimation of drifter dispersion thus clearly required that the drogue status of each drifter be known throughout the experiment. This paper reports on the algorithm used to separate drogued from undrogued drifters and to identify the time of drogue loss. Some verification of drogue status was possible in the field during the experiment. The resulting data were used to assess the proposed methodology.

Drogue loss is not a new drifter design challenge and has been encountered before in large drifter programs (Pazan and Niiler 2001; Poulain et al. 2009; Rio 2012; Lumpkin et al. 2013). Detection algorithms usually involve the separation of the effects of wind and waves and the shallow currents that they produce from the deeper ocean currents. The wind and wave effects on an SVP drifter drogued at 15 m and a CODE drifter drogued at 1 m has been found to increase from 0.1% of the wind speed for winds of up to $10\,\mathrm{m\,s^{-1}}$ when drogued (Niiler et al. 1995) to 1%–3% of wind speed without a drogue (Pazan and Niiler 2001; Poulain et al. 2009). Rio (2012) identified drogue losses of Surface Velocity Program (SVP) drifters in the Global Drifter Program. Wind/wave effects were identified using a combination of geostrophic velocity from altimetry and wind stress. Drogue loss was identified by an increase in wind slippage. Lumpkin et al. (2013) later improved on this method by also including changes in the transmission characteristics of drogueless drifters.

Unlike these large-scale programs, LASER sampled only a portion of the Gulf of Mexico (GoM) for only 2 months (Fig. 1b). A significant portion of the LASER drifters remained on the continental slope and shelf, where the geostrophic velocity is either weak or cannot be obtained accurately from altimetry. In the GoM interior, the temporal and spatial resolution of satellite altimetry is not sufficient to properly isolate the wind-induced component of the velocity. These factors limit the usefulness of altimeter-based methods for the LASER drifters.

However, changes in the transmission characteristics are observed as well with the CARTHE drifter when the stability of the floater is affected upon drogue loss, a property used in the algorithm described here. The high drifter density of the LASER drifter arrays compared to global arrays can also be exploited: Drogued and undrogued drifters clearly separate during storms, resulting in an easy classification for a big fraction of the drifter population. The long-lasting proximity of the drifters during most of the experiment allowed for a continuous comparison between neighboring drifter velocities, thus providing a powerful metric to detect both drogue status and times of drifter loss.

The algorithm described here has two major stages: First, populations of clearly drogued and undrogued drifters satisfying quantitative criteria of reduced data transmission and high cumulative downwind displacements are identified and confirmed visually using animations. Wind velocities to determine downwind displacements were taken from the Unified Wave Interface–Coupled Model (UWIN-CM; Chen et al. 2013), a fully coupled atmosphere–wave–ocean model. Second, the status of unclassified drifters is deduced by comparing their motions with those of nearby drifters with known drogue status. The drogue status of previously classified drifters is also verified this way. This

step is repeated iteratively, identifying increasingly more drifters at each step. Confirmation of drogue status at each step includes consideration of data transmission and visual inspection of animations.

The paper is organized as follows: The LASER data and the coupled model used for the wind and wave analysis are described in section 2. The methods for drogue-loss detection are explained in section 3. The results are presented in section 4, followed by a discussion and conclusions in section 5.

2. Data and model

a. CARTHE drifters

1) DESIGN

The CARTHE drifter (Fig. 1a) is 60 cm tall and composed of three parts: a donut-shaped floater housing a SPOT (https://www.findmespot.com) global positioning system (GPS) unit and alkaline batteries, four sails constituting the drogue, and a flexible rubber tube connecting the drogue to the floater. The flexible tube allows the floater to follow the tilting surface of waves and the drogue to remain more upright. This minimizes windage on the floater and advection of the drifter by the waves. Both the floater and the drogue are made of a biodegradable plastic. The drifter is therefore made of 85% biodegradable material, 10% of nontoxic (i.e., alkaline) batteries, and 5% electronics in its composition. Laboratory and field tests (Novelli et al. 2017) find that the drifter with a drogue follows the average Lagrangian velocity of the upper 60 cm. Without a drogue, it follows the upper 5 cm. In the presence of wind, the slip velocity is 0.5% of the 10-m wind speed with a drogue and 2% without a drogue.

2) LAUNCH OBJECTIVES AND CONFIGURATIONS

LASER began with a large-scale survey (LSS) of 37 drifters to document the mesoscale field and to help target areas for clustered releases. It was followed by three main launches of about 300 drifters each, including two localized quasi-instantaneous cluster launches and one designed to sample an evolving front (Fig. 2). Each of the large drifter deployments of LASER (Fig. 2a) had a different objective: The phase 1 (P1) deployment aimed to reenact part of the Grand Lagrangian Deployment (GLAD) of summer 2012 (Poje et al. 2014; Olascoaga et al. 2013; Berta et al. 2015; Curcic et al. 2016) under wintertime conditions. Submesoscale flows have a pronounced seasonality and are known to be more ubiquitous in the mixed layer in winter and fall (Mensa et al. 2013). The P1 launch (21 January) was centered at 29.05°N, 87.7°W and was contained in a 0.1° × 0.1° domain. A rapidly deployed cloverleaf pattern, consisting of nodes with drifter triplets and spanning an area about 7 km × 7 km, was designed to measure multiscale dispersion with roughly 300 drifters (Fig. 2b). The other semi-instantaneous launch was the large drifter array (LDA), which was focused on the evolution of a submesoscale dipole using a rectangular array of more than 300 drifters, with 1-km spacing, spanning an area about 16 km × 19 km (Fig. 2d). The LDA cluster (7 February) was centered at 28.9°N, 88.45°W close to the Mississippi River outflow in a 0.15° × 0.15° box. A vortex line deployment consisting of 19 drifters, which followed the LDA release within less than 2 h, is grouped with the LDA launch for the purposes here. The phase 2 (P2) deployment aimed to follow the evolution of a surface front on the edge of a Mississippi River plume. This front was adaptively reseeded as drifters dispersed along the convergence zone (Fig. 2c). The P2 launch (25–31 January) covered a wider area of 28°–29°N, 88°–88.7°W, as it followed the evolution of a front of Mississippi River water advecting into the GoM interior. In addition, drifters were released in conjunction with many hundreds of bamboo plates, photographed from an aerostat, as part of phase 3 (P3). This part of the experiment sought to study the small-scale (tens of meters) Langmuir circulation and frontal convergences. To optimize the placement of each deployment, survey lines of drifters were also released. The P3 launches (four releases of three to nine drifters) occurred mostly during the P2 experiment in the same area. For this reason they are included in the P2 group in this study as are short survey line releases around this time. Finally, the last release ("test") aimed to address the drogue-loss issue, which had become apparent by then. All of these deployments resulted in drifter arrays with many drifter–drifter separations of only a few kilometers. The drifters remained in close proximity for several weeks. This was particularly true for those in the NGoM, where the geostrophic component of the velocity is weak. Although the wind exerted a strong influence on the drifter motion, increasing the speed, it did not increase dispersion.

b. UWIN-CM

The source for the synoptic wind and wave data used in this study is the UWIN-CM (Chen et al. 2013; Chen and Curcic 2016). It is designed as a multimodel system with the flexibility to exchange individual model components for the atmosphere, waves, ocean, land, and sea ice. The model has been used to study the role of the Stokes drift in surface transport (Curcic et al. 2016), the impacts of coupling on boundary layer structure in Hurricane Isaac in 2012 (Zhu et al. 2016), and the atmospheric forcing's influence on the transport in the Gulf of Mexico on diurnal and seasonal scales (Judt et al. 2016). Here, the

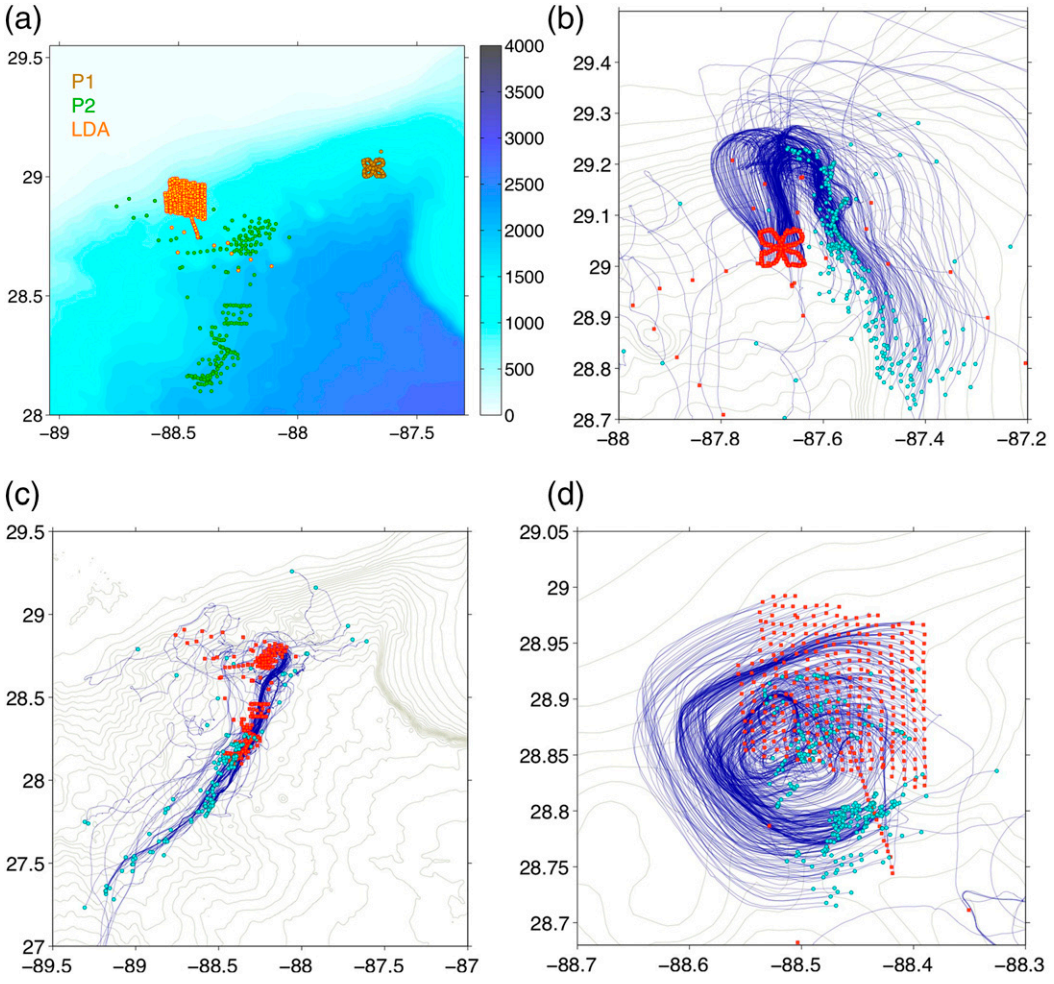

FIG. 2. (a) The launch locations of the three major clusters: P1 (in brown), P2 (in green) and LDA (in orange). The launch configurations (red) of (b) P1, (c) P2, and (d) LDA, superimposed on isobaths at 100-m intervals. Trajectories are shown for 2.7, 7.3, and 1.8 days for P1, P2, and LDA, respectively (last positions marked in cyan).

system consists of fully coupled atmosphere, surface wave, and ocean circulation models.

The atmosphere model is the nonhydrostatic Weather Research and Forecasting (WRF) Model, version 3.7.1, with the Advanced Research version of WRF (ARW) dynamical core (Skamarock et al. 2008). WRF is configured with 36 vertical layers and a 12-km horizontal resolution on the domain (7°–45°N, 103°–55°W), with a 4-km resolution nest covering the entire GoM.

The surface wave model is the spectral University of Miami Wave Model (UMWM), version 2 (Donelan et al. 2012). It is configured with 4-km grid spacing on the inner WRF nested domain. The wave energy spectrum is represented by 36 directional bins and 37 frequency bins that range from 0.0313 to 2 Hz on a logarithmic scale.

The three-dimensional Stokes drift fields (Stokes 1847; Phillips 1977) for this study are evaluated by computing the full integral over the wavenumber directional space:

$$\mathbf{u}_{\mathrm{St}} = \int_0^{2\pi}\int_0^{\infty} \omega k^2 \frac{\cosh[2k(d+z)]}{2\sinh^2 kd} F(k,\theta)\, dk\, d\theta, \quad (1)$$

where ω is the angular frequency, k is the wavenumber, d is the mean water depth, z is the distance from the surface (negative—downward) at which the Stokes drift field is being evaluated, F is the wavenumber energy spectrum, and θ is the direction of the waves.

The ocean circulation model is the Hybrid Coordinate Ocean Model (HYCOM), version 2.2 (Wallcraft et al. 2009), with full tidal forcing. It is a three-dimensional hydrostatic ocean model with hybrid vertical coordinates: z levels in shallow water, terrain-following coordinates in intermediate water, and isopycnal

(constant density) coordinates in deep water. HYCOM is configured with 0.04° (roughly 4 km) horizontal grid spacing and 32 vertical levels on the WRF outer domain.

The coupling is implemented using the Earth System Modeling Framework (ESMF; Hill et al. 2004). Fields between all components are exchanged every 60 s. Initial and lateral boundary conditions were taken from the National Centers for Environmental Prediction (NCEP) Global Forecasting System (GFS) daily forecasts at 0.25° horizontal resolution for WRF and from the global, data assimilating, 0.08° horizontal-resolution daily HYCOM fields for the ocean model.

Daily 72-h real-time forecasts were generated from 1 January 2015 to 1 April 2016. Each daily forecast is initialized from GFS and global HYCOM fields for the atmosphere and ocean components, respectively. The wave model is initialized from the previous day's forecast. After spinup time from the initialization of the global model to the atmosphere model (WRF) during which storm-scale features develop, the 24–48 h of each forecast are concatenated to obtain continuous fields of surface wind and Stokes drift during the LASER drifter analysis period.

3. Methods for drogue-loss detection

Following an initial preprocessing of the drifter trajectories, the first stage of the drogue-status classification scheme consists of defining populations of "obviously" drogued and undrogued drifters, characterized by their GPS transmission rate and cumulative downwind displacements (see sections 3b and 3c). In the second stage, which requires a predefined population of nearby drifters of known status, relative velocities and relative motion comparisons are carried out to identify drogue losses for the remaining drifters, as well as refining and/or correcting the status of the first guess. This process is repeated multiple times, until almost all of the drifters are classified. Both stages heavily rely on the surface wind and Stokes drift estimates from the UWIN-CM. The second stage exploits the long-lasting clustering of the drifters.

a. Trajectory preprocessing

Drifter positions are nominally reported every 5 min, with a nominal accuracy of about 7 m. Minimal quality control is performed initially on the drifter trajectories. First, any measurement implying a drifter velocity above $2\,\mathrm{m\,s^{-1}}$ is removed. Then, the drifter trajectories are linearly interpolated to regular 15-min intervals, starting on 18 January 2016. Velocities are estimated from forward differences on the interpolated positions, thus representing an average velocity over that time interval. The time interval between measurements, Dt_{15}, associated with each of the interpolated positions is set equal to the nearest-in-time transmission gap of the raw data stream, Dt, for the specific drifter. A consequence of this formulation is an emphasis on the outliers, since a large Dt will be counted several times ($\sim Dt/15$ times). This aids in the identification of periods of GPS anomalies.

b. GPS transmission rate

The drogue loss during LASER clearly had an impact on the GPS transmission rate. The team on site noticed that in the presence of large waves, the floaters without drogues tended to flip upside down, pointing the satellite antenna downward, and then flip again, pointing it upward. This reduced the frequency of transmissions, but it did not suppress them completely. Note that this trend is specific to the CARTHE drifter and contrary to the SVP drifter, which tends to transmit more frequently in the absence of drogue (Lumpkin et al. 2013). The transmission rate was reduced for all drifters during storms, perhaps as a result of additional motion of the drifter and the occasional submergence of the floater. The time interval between measurements Dt has a median of 5 min for both drogued and undrogued drifters. Yet, the number of outliers is markedly higher for the undrogued ones. For instance, we find 4.8% of $Dt > 15$ min for the undrogued versus only 0.05% for the drogued drifters, 2.01% versus 0.01% of $Dt > 30$ min, and 0.66% versus 0% of $Dt > 1$ h. Note that in spite of the skewness toward $Dt > 5$ min, the median remains at 5 min because almost 80% of Dt values are between 4.5 and 5.5 min for both populations. It is clear that the programmed 5-min interval remains the dominant signal for both categories, while the outliers mark the next successful attempt at transmitting, and their probability distribution function (pdf) is therefore discretized (not shown) with normal distributions at every 5-min interval. One can see, then, that counting outliers in the time series can help identify the drogue state of portions of trajectories. However, it does not always prevent confusion with a wind event affecting as well the transmission of drogued drifters, resulting in only a vague estimate for the drogue loss. The approach here is to emphasize the outliers by relying on Dt_{15} and then detecting their sudden appearance with the time derivative.

A metric for detecting large local changes in Dt_{15} is defined as

$$Q(n, t_k) = \langle |\Delta Dt_{15}| \rangle_{5\mathrm{hr}}, \tag{2}$$

where n is the drifter number, t_k is the kth time, ΔDt_{15} is the difference between consecutive values of Dt_{15}, and $\langle\,\rangle_{5\mathrm{hr}}$ denotes a 5-h average centered on t_k. The 5-h low pass on the gradient of Dt_{15} further spreads in time the changes in transmission while removing anomalies, as illustrated in Fig. 3a: Q displays areas of high values that correspond to specific events of high winds and/or waves

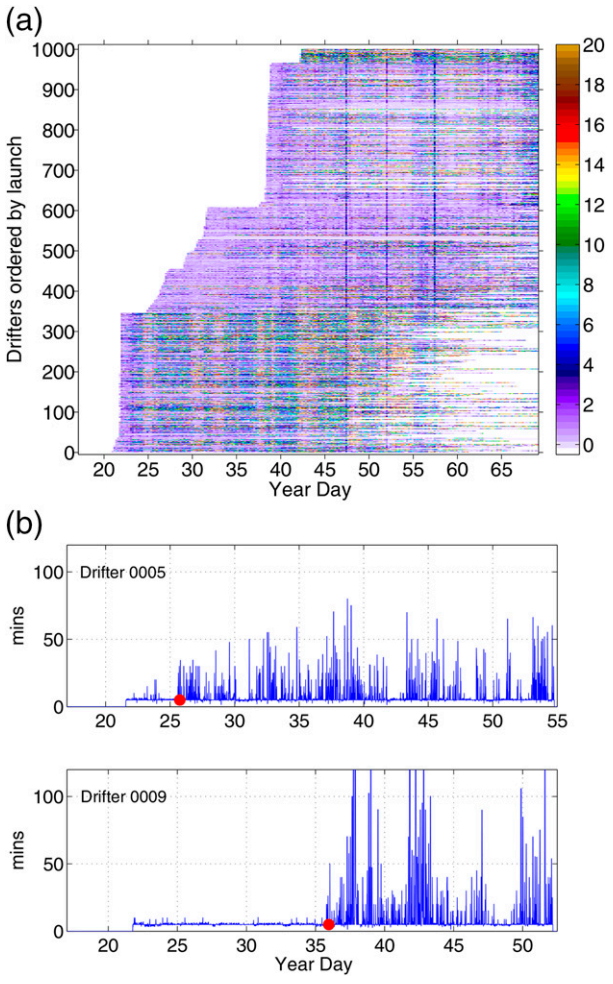

FIG. 3. (a) The values of Q (min) computed for the drifter array until 8 Mar. The color scale is saturated at 20 min. (b) Time series of Dt_{15} for drifters 0005 and 0009. The estimated time of drogue loss from the algorithm described in section 3 (red dots).

(light brown). Additionally, slightly higher values among the moderately low Q are the signatures of undrogued drifters (cyan and green). A predominance of this signal is seen for the drifters up to ≈420—that is, from the P1 launch—and for those ~1000 from the test launch. Undrogued drifters are characterized by a high occurrence of Q values longer than 5 min. Note also the presence of three vertical lines between yeardays 45 and 60, which most likely correspond to a glitch in the satellite transmission system. After several tests involving drifter animations, it was estimated that more than five occurrences of those high ($Q > 5$ min) values before 9 March give a reasonable guess of the undrogued status. Indeed, this first estimate successfully differentiated between the groups of drifters with different advection types among the cloverleaf and LDA clusters. The time of drogue loss is then approximated by the first instance of those Q regimes. Figure 3b shows how the algorithm identifies the change in Dt_{15} regime for drifters 0005 and 0009. Note that this estimate is approximate and used only as a first guess. Other algorithms on the Dt distribution can produce different drogue-loss dates. Nevertheless, the Q criterion was confirmed in a later stage of the analysis to estimate reasonably well (within a few days) the times of loss for a large fraction of the major clusters.

c. *Surface wind and Stokes drift contribution*

The drogued CARTHE drifter follows the flow integrated over the top 0.6 m, but the flow in the first few centimeters is more affected by the wind and the Stokes drift. The undrogued drifter motion has therefore a stronger wind- and wave-driven component than the drogued drifter motion. Additionally, there could be some wind slip resulting from having part of the floater above the water (Novelli et al. 2017). The surface wind field is thus used to help distinguish between drogued and undrogued drifters. The 10-m wind magnitude of the UWIN-CM hourly output is interpolated to the LASER drifter positions. Figure 4a illustrates the surface wind as felt by the drifters, which is characterized by vertical bands of high and low magnitudes corresponding to the synoptic or large-scale signature of the wind patterns in the northern Gulf of Mexico. The surface Stokes drift magnitude (Fig. 4b) displays close similarities with the wind data, in particular for the major wind events. This is not surprising considering that the waves are mostly generated by strong winds at this time of the year. In particular, the enclosed geometry of the Gulf of Mexico appears to ensure that wind and waves are almost always strongly correlated with one another, as a result of the absence of remotely generated swell. The major wind events in decreasing order occur on 22 January (a day after the P1 launch), 24 February (yearday 55), 9 February (yearday 40, not long after the LDA launch), 9 March (yearday 68), 5 February (yearday 36), 28 January, 19 February (yearday 50), and 15 February (yearday 46).

The combined direct and indirect effects of the surface wind on any drifter trajectory can be estimated by calculating the cumulative displacements downwind and crosswind (the latter for comparison purposes). Of course, other forces may align with the wind occasionally, and these cannot be distinguished by this method. The Lagrangian velocities in the wind reference frame become

$$\mathbf{V}_{\text{proj}}(n,t) = \mathbf{V}(n,t) \cdot \mathbf{V}_{\text{wind}}(n,t)[\mathbf{V}_{\text{wind}}(n,t) \cdot \mathbf{V}_{\text{wind}}(n,t)]^{-1}\mathbf{V}_{\text{wind}}(n,t), \quad (3)$$

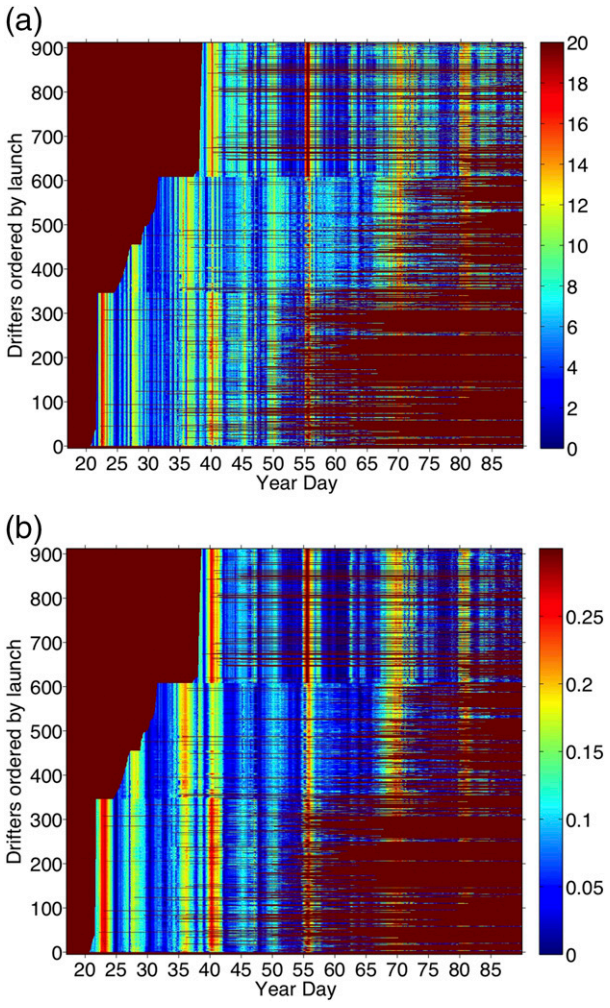

FIG. 4. (a) The 10-m wind and (b) surface Stokes drift magnitudes ($\mathrm{m\,s^{-1}}$) interpolated to the drifter array. No data transmission before the launch and once drifters stop emitting (dark red pixels) are also indicated.

$$\mathbf{V}_{\mathrm{rej}}(n,t) = \mathbf{V}(n,t) - \mathbf{V}_{\mathrm{proj}}(n,t), \tag{4}$$

where $\mathbf{V}(n, t)$ is the velocity of the drifter n at time t, $\mathbf{V}_{\mathrm{wind}}(n, t)$ is the surface wind vector at the drifter's location, and $\mathbf{V}_{\mathrm{proj}}$ and $\mathbf{V}_{\mathrm{rej}}$ are the projection (downwind) and rejection (crosswind), respectively, of $\mathbf{V}$ onto $\mathbf{V}_{\mathrm{wind}}$.

The total downwind displacement can be computed as

$$L_{\mathrm{proj}}(n) = \sum_{k=1}^{N_n} \left|\mathbf{V}_{\mathrm{proj}}(n,t_k)\right| \Delta t, \tag{5}$$

where $\Delta t = 15\,\mathrm{min}$ and the sum is taken over the entire length of each trajectory to account for different launch times. From this, an average downwind cumulative velocity is derived as

$$\langle|\mathbf{V}_{\mathrm{proj}}(n)|\rangle = \frac{1}{N_n \Delta t} L_{\mathrm{proj}}(n). \tag{6}$$

Similarly, the average crosswind cumulative velocity is

$$\langle|\mathbf{V}_{\mathrm{rej}}(n)|\rangle = \frac{1}{N_n \Delta t} L_{\mathrm{rej}}(n) = \frac{1}{N_n} \sum_{k=1}^{N_n} |\mathbf{V}_{\mathrm{rej}}(n,t_k)|. \tag{7}$$

A similar decomposition can be made in the reference frame of the surface Stokes drift. Assuming that the drifter trajectories are either mostly drogued or mostly undrogued, the presence of both populations should lead to a bimodal pdf for $\langle|\mathbf{V}_{\mathrm{proj}}|\rangle$, while the distribution remains normal for $\langle|\mathbf{V}_{\mathrm{rej}}|\rangle$. The undrogued drifters are most likely represented by the local distribution with the larger local maximum and the opposite for the drogued drifters. A first guess of the drogue status can then be made by setting a critical value between the two maxima separating the drogue categories. There are a couple of reservations about $\langle|\mathbf{V}_{\mathrm{proj}}|\rangle$: First, if the drogue loss times are randomly distributed, then an ensemble of different segments of drogued and undrogued portions of trajectories could mask the bimodal distribution. However, the semisynchronized drogue losses from the cloverleaf and LDA groups occurring shortly after their launches prevented that bias. Second, as the drifters disperse, they get entrained by different circulation features with velocity magnitudes potentially masking the contribution of the wind. Computing the cumulative displacement in the GoM interior is therefore problematic because of the highly kinetic geostrophic currents. Nevertheless, this is the best metric we found. The instantaneous downwind displacement time series or correlations with the wind and waves, for instance, did not leave any clear signature allowing for distinction between drogued (DD) and undrogued (UD) drifters.

d. Relative velocities

Drifters that meet criteria based on the considerations described in sections 3b and 3c are sorted into preliminary groups of DD and UD drifters; the remaining drifters, for which these two tests are inconclusive, are left in an "unknown" (UU) group. The UU drifters essentially fall into two categories: nominal GPS transmission with large $\mathbf{V}_{\mathrm{proj}}$ and anomalous GPS transmission (and drogue-loss estimated time) with low $\mathbf{V}_{\mathrm{proj}}$. Drogued drifters can easily fit the first category if they have been entrained in the GoM interior, where mesoscale flows increase substantially the cumulative displacement, while undrogued drifters can fit the second category if the drogue-loss time is an outlier. The velocity of any UU drifter can then be directly compared

to nearby DD and UD drifters. This approach is based on the assumption that for drifters separated by less than the radius of deformation, horizontal differences in the background flow are small during wind events compared to the differences in depth-integrated velocities between the top 5 cm and the top 60 cm. Therefore, comparing a UU drifter's velocity to each of the two neighboring groups of DD and UD drifters can indicate to which drogue category it belongs at a particular time. This is true particularly on the continental shelf and slope, where the geostrophic velocities are weak. In the GoM interior, the horizontal gradients of the mesoscale circulation are more pronounced, so velocity comparisons of nearby drifters do not necessarily isolate the wind and wave contribution.

Consider the common configuration sketched in Fig. 5a: At a certain time t, a drifter n is surrounded by and in close proximity to several DD and UD drifters. Its projected velocity $\mathbf{V}_{\text{proj}}(n, t)$ can be compared to those of the surrounding drifters within a specified distance (gray disk) by defining two averaged velocity differentials—one for the drogued population, $\Delta V^{\text{DD}}(t)$, and one for the undrogued population, $\Delta V^{\text{UD}}(t)$—as

$$\Delta V^{\text{DD}}(t) = \left[\overline{|\mathbf{V}_{\text{proj}}(i\text{DD}, t) - \mathbf{V}_{\text{proj}}(n, t)|^2}\right]^{1/2}, \quad (8)$$

and

$$\Delta V^{\text{UD}}(t) = \left[\overline{|\mathbf{V}_{\text{proj}}(j\text{UD}, t) - \mathbf{V}_{\text{proj}}(n, t)|^2}\right]^{1/2}, \quad (9)$$

where the overbar denotes the average over all nearby drogued (with indices iDD) or undrogued (with indices jUD) drifters. The projection can be done onto the wind or the Stokes drift (Fig. 4). Here we chose the Stokes drift because it has fewer high-frequency spikes. The resulting time series are expected to show a pattern similar to the idealized representation in Fig. 5b. If a drifter is undrogued, then its velocity is closer to those of the nearby UD drifters, whereas it differs significantly from those of the nearby DD drifters. A sustained $\Delta V^{\text{UD}}(t) < \Delta V^{\text{DD}}(t)$ is therefore an indication that the drifter is undrogued. On the other hand, $\Delta V^{\text{UD}}(t) > \Delta V^{\text{DD}}(t)$ means that the drifter is still drogued. The change between these regimes, where the curves for ΔV^{DD} and ΔV^{UD} cross, occurs at the time the drogue detaches from the floater, marked in Fig. 5b by the dashed line at time t^L. When the nearby DD and UD populations are large, t^L can be determined to within a half hour. On the other hand, when they are small, this test may be inconclusive.

e. Visual analysis

When a UU drifter is surrounded by other drifters from the known populations, it is possible to visually identify the drogue status from its advection/displacement relative to the other nearby drifters. Lagrangian animations (i.e., animations centered on a drifter) are used for each drifter to confirm the drogue-loss dates estimated from $\Delta V^{\text{DD}}(t)$ and $\Delta V^{\text{UD}}(t)$ and to define the time after which a drifter's DD status becomes uncertain (essentially when insufficient nearby drifters remain for a meaningful comparison). The animations complement the ΔV metric, in particular when the number of nearby drifters is too small to provide statistically reliable ΔV estimates.

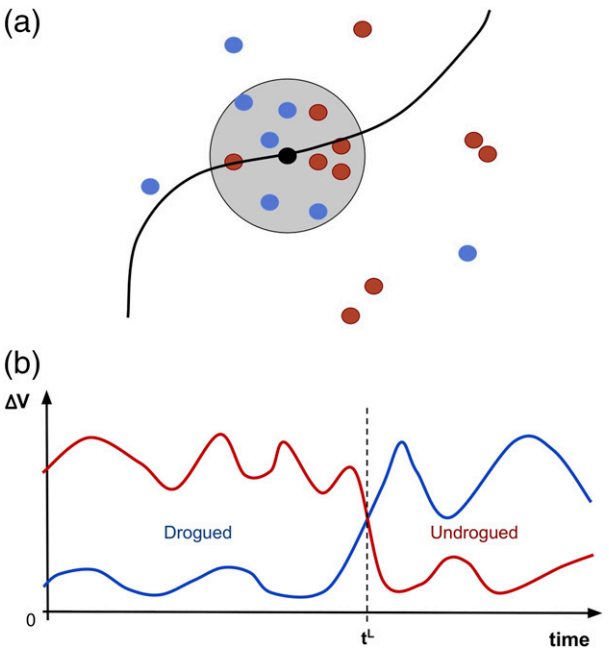

FIG. 5. (a) A schematic diagram showing a drifter trajectory and its position at a given time (black dot), surrounded by DD (blue dots) and UD (red dots) drifters. The DD and UD drifters in the gray disk (with a radius of either 0.1° or 0.2°) are used to calculate the averaged velocity differences ΔV^{DD} and ΔV^{UD}. (b) A representation of $\Delta V^{\text{DD}}(t)$ (blue line) and $\Delta V^{\text{UD}}(t)$ (red line) as a function of time for a drifter losing its drogue at the time t^L (dashed line).

f. Filtering

After the drogue-status analysis was complete, the drifter positions were filtered and edited to produce the final dataset, using the method developed by Yaremchuk and Coelho (2015). It is a variational method providing a realistic approximation of the acceleration while keeping the difference between the filtered and observed trajectories within the error bars of the position uncertainty. The filter was applied previously to the GLAD dataset and successfully cleaned the data without smearing. Tests on metrics particularly sensitive to noise in the Lagrangian relative velocities, such as the scale-dependent

finite-scale Lyapunov exponent (FSLE) and the structure function (Poje et al. 2014), confirmed its ability to preserve the small-scale motions. D'Asaro et al. (2018) show that it is equivalent to a low-pass filter with a cutoff of about 10^{-4} Hz. They also show that it effectively removes GPS errors.

4. Results

Both stage 1 (sections 3b–c) and stage 2 (sections 3d–e) of the drogue analysis are conducted for the first 7 weeks of LASER until 8 March while the drifters are still clustered. The drogue detection is then extended by 3 weeks, as described in section 3c, to provide margins of error and to take advantage of a late clustering near the shoreline.

a. Stage 1

In stage 1 the onset of GPS transmission anomalies is assumed to coincide with the drogue detaching from the floater (cf. section 3b). The estimated times of drogue loss t^L based on the metric Q in Eq. (2) are displayed in Fig. 6a. The average wind speed as felt by the drifters is plotted in Fig. 6b. The LSS and P1 groups (first 346 drifters) sustained the highest number of drogue losses (about half) within a day or two of their releases, which corresponds to the major storm event of 23 January. The LDA group (launches 623–967) also lost a significant number of drogues within the first 2 days postlaunch, timed with another wind event around 9 February (yearday 40). For P2 (launches 347–622), the losses are more evenly distributed over time. The last group (launches 968–1001) was released during tests where several drifters were purposefully launched without drogues.

Overall, by 8 March (yearday 67) an estimated 447 out of 1001 drifters were found to have lost their drogues. Note that this first guess depends on the number of occurrences of $Q > 5$ min chosen as the threshold. If that number is increased, then the UD population is reduced. The final drogue status obtained by the recursive procedure of stage 2 was found not to be sensitive to this parameter.

Next, the effect of wind and waves is considered (cf. section 3c). As anticipated, the distribution of $\langle|\mathbf{V}_{\text{proj}}|\rangle$ is clearly bimodal (Fig. 7b), with the first local maximum at about 17 cm s^{-1} and the second at 27 cm s^{-1}. On the other hand, $\langle|\mathbf{V}_{\text{rej}}|\rangle$ has a normal distribution centered around 17 cm s^{-1}, which is the same as the lower maximum of $\langle|\mathbf{V}_{\text{proj}}|\rangle$. The departure from the typical near-Gaussian distribution is a clear indication that two regimes of advection are captured by the LASER drifters: Those with high $\langle|\mathbf{V}_{\text{proj}}|\rangle$ are most likely drogueless, and those with lower $\langle|\mathbf{V}_{\text{proj}}|\rangle$ are assumed to remain drogued. However, this classification is imperfect. Faster downwind velocities can also result from geostrophic flows that happen to align with the direction of the wind. This is the case for most of the P2 group, when the drifters were released along a front (cf. Figs. 7a,c). Additionally, randomly distributed drogue losses can mask the bimodal distribution, although it is not the case here, since the cloverleaf and LDA groups account for the massive quasi-synchronized drogue losses. Nevertheless, the separation between drogued and undrogued drifters is assumed to occur at a value of $\langle|\mathbf{V}_{\text{proj}}|\rangle$ at the local minimum of the bimodal distribution between the two local maxima, at $\approx$22.5 cm s^{-1}. For the trajectories through 8 March, 429 drifters are found with $\langle|\mathbf{V}_{\text{proj}}(n)|\rangle \geq 22.5$ cm s^{-1}. Note that while this metric helps identify drifters that lost their drogue at some point, it does not provide estimates of drogue-loss times.

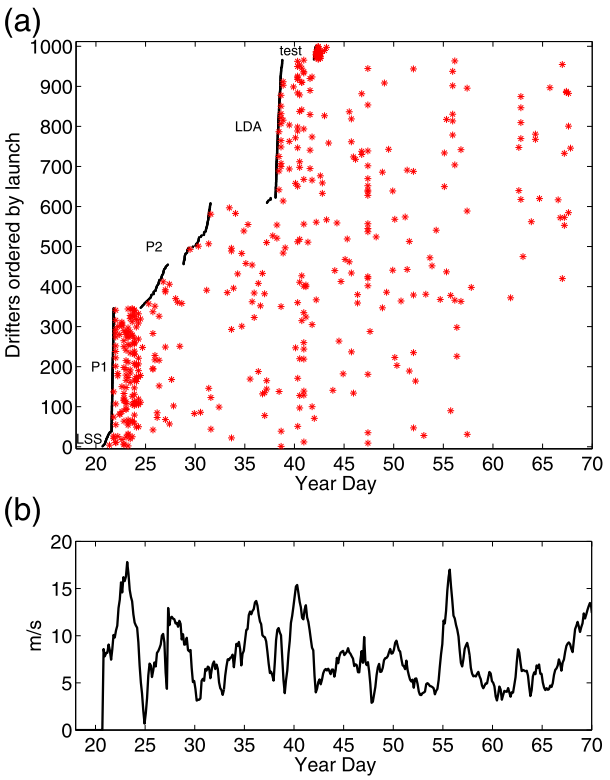

FIG. 6. (a) The estimated time of drogue loss from GPS transmission (red stars) vs drifter identification numbers reordered chronologically by their launch dates (black dots). The different launches are identified in the figure, including the LSS, P1, P2, LDA, and test deployments (cf. Fig. 2). (b) Time series of the wind felt on average by the drifters.

A reasonable first guess for stage 1 can now be obtained by combining the estimates from the two metrics. A drifter is assumed UD at a given time if the GPS transmission is unusual (as defined by the Q

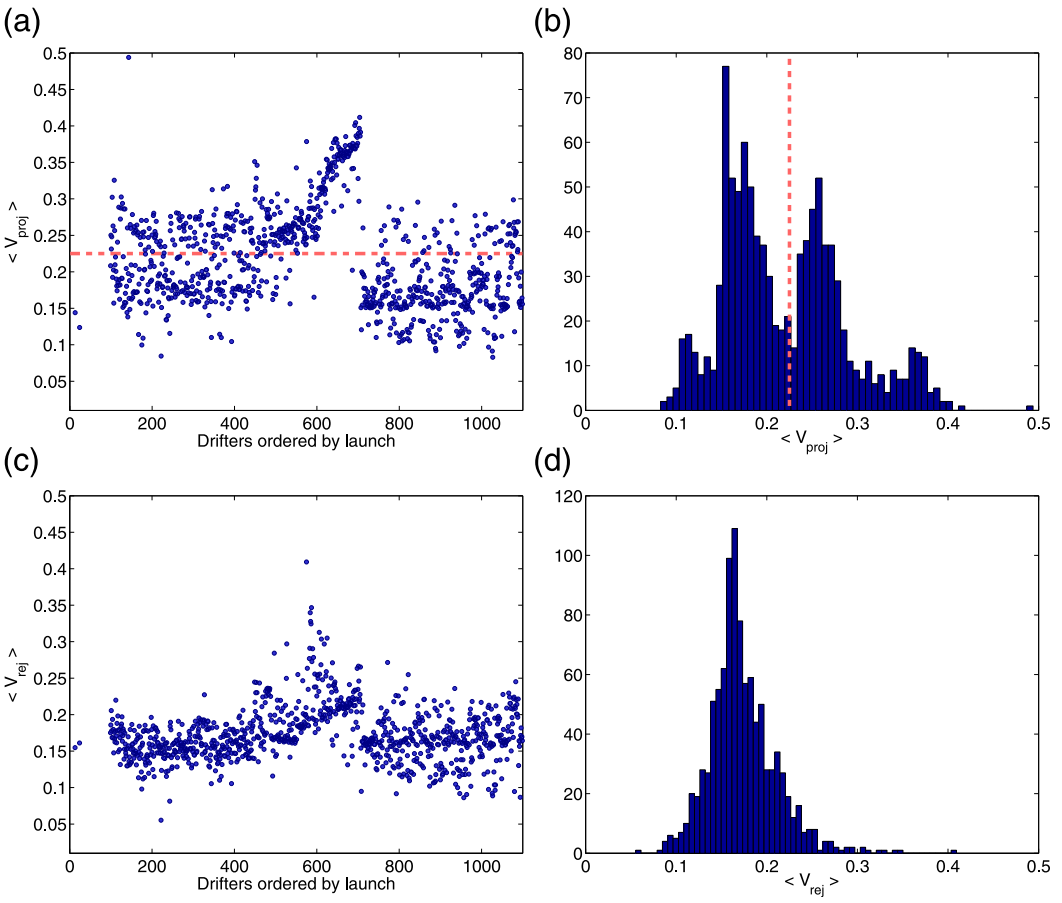

FIG. 7. (a) The average downwind velocity ($m\,s^{-1}$) for each drifter. (b) Histogram of (a). The separation at $22.5\,cm\,s^{-1}$ between the assumed drogued and undrogued categories (red dashed line) is marked. (c),(d) As in (a) and (b), respectively, but for crosswind velocities.

criterion) and if $\langle|\mathbf{V}_{proj}(n)|\rangle \geq 22.5\,cm\,s^{-1}$, and conversely a drifter is assumed DD at a given time if $\langle|\mathbf{V}_{proj}(n)|\rangle < 22.5\,cm\,s^{-1}$ and the GPS transmission is normal.

At this stage of the analysis, we ignore both GPS batteries' end of life and future changes of drogue status (from DD back to UU when drifter density is too low) when calculating the ensemble in each drogue category. These "cumulative numbers" allow for keeping track of the progress in drogue-loss detection. Figure 8 shows the cumulative numbers in each of the three drogue categories: DD, UD, and UU. The number of DD drifters is seen to jump up at every cluster launch and then slowly decrease over time, while the number of UD drifters keeps increasing, with leaps corresponding to strong wind events. By 8 March, the cumulative numbers of DD and UD drifters are 382 and 257, respectively, out of a total of 1001, and the number of UU drifters reaches 362, about a one-third of the drifter dataset (cf. Table 1).

Inspection of the drifter distributions a few days after each launch in Fig. 9 shows a spatial separation of the drogued and undrogued drifters for the P1 and LDA launches resulting from their different velocities. While this gives confidence in the stage 1 procedures, the classification is still imperfect. The P2 group does not show a similar pattern. Unlike P1 and LDA, the drifters were released in a broad region along the front over many days, so a clean geographical distribution is not expected. This release also has the least drogue loss (cf. Fig. 6). Furthermore, the strong currents in this region bias the stage 1 displacement classification toward undrogued drifters, even though the GPS transmission rate remained high. Thus, for the P2 group, the transmission rate criterion is likely the more reliable metric.

As summarized in Table 1, out of those 362 UU drifters, 172 with normal transmission and high average downwind velocity are most likely drogued drifters sampling the geostrophic currents aligned with the wind. The majority of drifters originate from the P2 launch. The other 190 UU drifters with bad transmission and low average downwind velocity probably

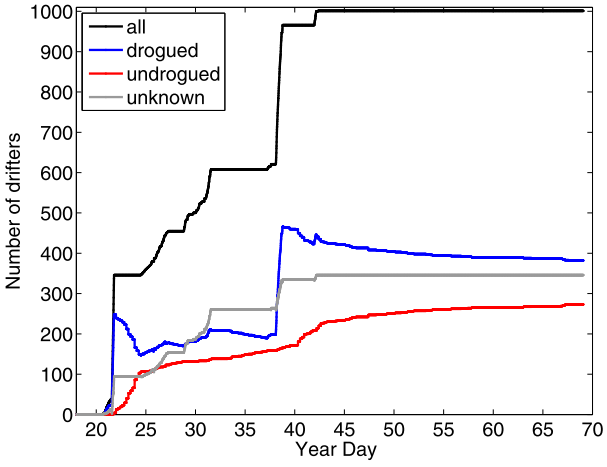

FIG. 8. Stage 1, first-guess estimate of the cumulative number of launched drifters that still have their drogues (blue), that lost their drogues (red), and of unknown status (gray) as a function of time. The total number of drifters launched is also plotted (black).

lost their drogues, although it occurred either at a later time than the massive drogue losses or the drifters had average downwind velocities near the threshold between the DD and UD groups.

Overall, we conclude that at the end of stage 1, two-thirds of the drifters are assigned a drogue status consistent with their spatial distribution. More importantly for the next stage of the analysis, the remaining UU drifters are mostly embedded in the known population clusters; which sets the stage for a relative velocity comparison as described in section 3d.

b. Stage 2

During strong winds in the NGoM, the drogued drifters move differently than the undrogued drifters. The difference is most easily attributable to drogue status when the drifters are close together, so the variations in the underlying currents across the drifter array are small. The unique advantage of this dataset is the combination of frequent storms with the persistent clustering of UU drifters within close range of the known DD and UD populations.

An example of the stage 2 metrics is shown in Fig. 10 for drifter 0711. Its status was UU after stage 1 because $\langle|\mathbf{V}_{\mathrm{proj}}(711)|\rangle < 22.5\,\mathrm{cm\,s^{-1}}$, while anomalous GPS transmission was observed starting around 6 February (red disk at yearday 38.45 in Fig. 10a). It was then identified as UD during stage 2. Quantities $\Delta V^{\mathrm{UD}}(t)$ and $\Delta V^{\mathrm{DD}}(t)$ are computed every 15 min and then low-pass filtered with a 10-h moving average to remove the high-frequency variability (Figs. 10b,c). Also, 95% confidence intervals are computed using a bootstrapping method and plotted when at least 10 drifter neighbors

TABLE 1. Stage 1's cumulative number of drifters by 8 Mar 2016, belonging to the DD, UD, and UU categories, based on the estimates from GPS transmission gaps and average downwind velocities. Note: "bad" transmission refers to high occurrences of $Q >$ 5 min, while "low" and "high" refer to average downwind velocity below and above 22.5 cm s^{-1}, respectively.

Transmission	Avg downwind velocity	Status	Total No. of drifters
Good	Low	DD	382
Bad	High	UD	257
Bad	Low	UU	190
Good	High	UU	172

were identified in that group. The curves are discontinuous in some places as a result of the absence of drifters within a 0.1° radius. These gaps are reduced with a 0.2° radius (cf. Fig. 10d). Clear trends can be observed: $\Delta V^{\mathrm{UD}} > \Delta V^{\mathrm{DD}}$ until at least yearday 52; thus, the drifter has a drogue until at least 21 February. Then the reverse trend is observed at later times, indicating that it became undrogued. The crossing is not as neat and clear for the actual data as suggested by the schematic in Fig. 5b. Still, a most likely time of drogue loss can be determined as the time separating the regime when typically $\Delta V^{\mathrm{UD}} > \Delta V^{\mathrm{DD}}$ from that when typically $\Delta V^{\mathrm{DD}} > \Delta V^{\mathrm{UD}}$. For this drifter, this time t^L is 0600 UTC 24 February (yearday 55.37). The Q criterion was clearly misleading in this case as a result of the many outliers seen in the Dt_{15} time series prior to this date. Instead, t^L coincides with the onset of more sporadic transmission starting around yearday 55.

In the first iteration of stage 2, the ΔV curves are computed for each UU drifter of the dataset. Most of the UU drifters from the P2 launch are confirmed at this point to be still drogued. Overall, by 8 March the number of DD and UD drifters are increased during this step to 582 and 327, respectively, while the number of UU drifters is reduced to 92, that is, less than 10% (cf. stage 2a in Table 2).

The advantage of the ΔV metric is that it responds immediately to drogue loss, provided the drifter is surrounded by known populations at that time, and can narrow down the time of drogue loss to <1 h in optimal conditions. The wind and wave states are usually sufficient to differentiate between DD and UD motions, unless the wind dies down completely. In the latter case, the ΔV curves of both states will be similar until the wind picks up again. The weakness of this metric is its strong dependence on the prior sorting, as any error in a drogue state estimate potentially propagates to the next stage of detection. However, this problem is mitigated by the drifter density: It would require more than one isolated misdiagnosed case to impact the statistics. The angle

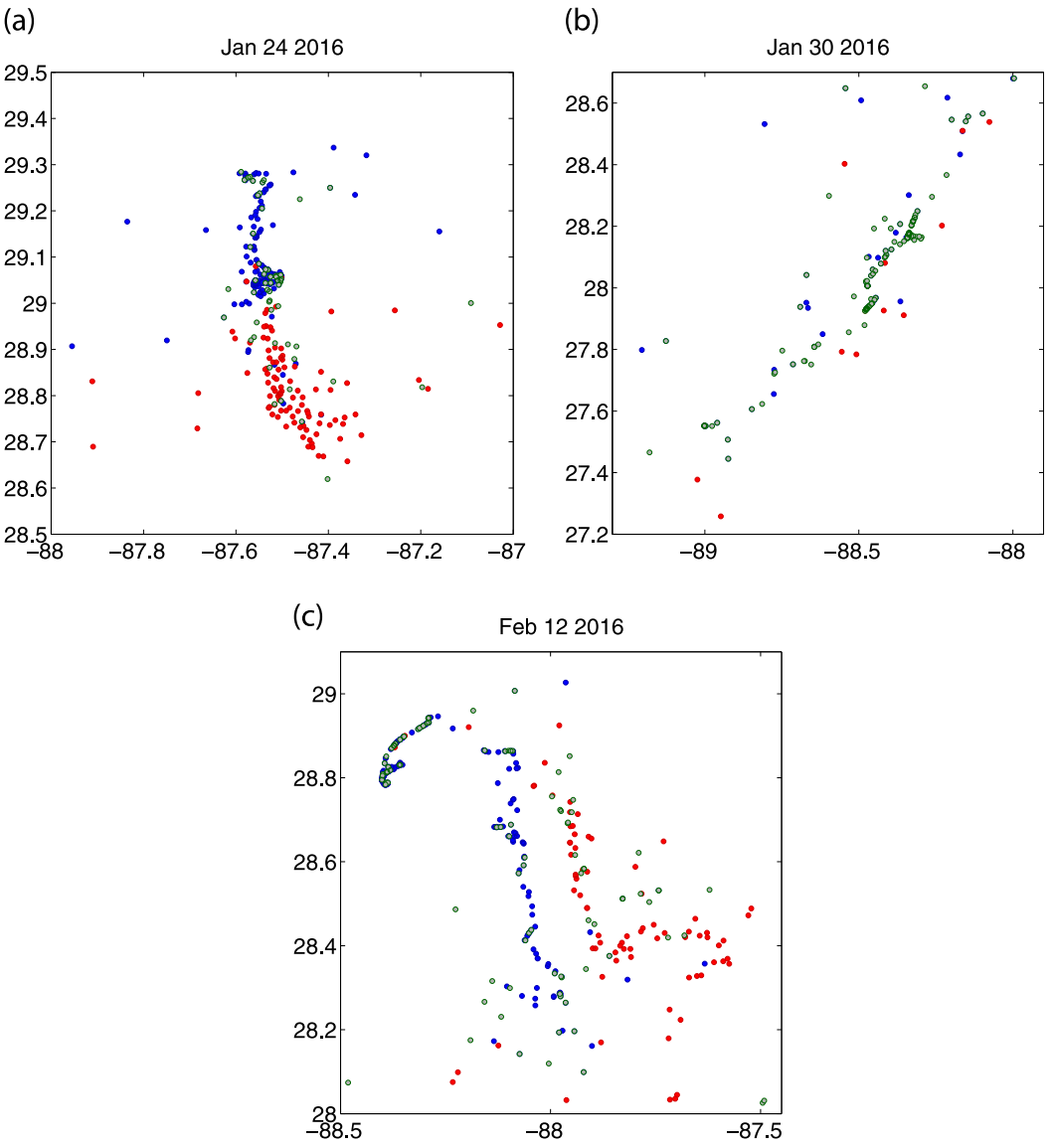

FIG. 9. The drifter distributions at the end of stage 1 for the three main launch groups—(a) P1, (b) P2, and (c) LDA—a few days after their release. The DD (blue), UD (red), and UU (gray) drifters are plotted.

differential between the wind and the drifter velocities is also indicative of the drogue state (not shown). For instance, the direction of displacement of an undrogued drifter is closer to the wind direction than it is for the nearby drogued drifters. This metric was found to be less precise than ΔV in detecting drogue-loss times, but it could be used in conjunction with ΔV when there are insufficient drifters nearby.

Resolving the drogue status of an additional 270 drifters in the first iteration of stage 2 improved substantially the population densities for a second sweep. The values of $\Delta V(t)$ are recalculated for all drifters through 8 March. The previously estimated times of drogue loss t^L are then corrected or adjusted if necessary, and the populations of DD and UD drifters are updated.

Two other generic examples of GPS transmission rate and relative velocities are provided in Fig. 11, for both a DD and a UD drifter from the P1 launch. Both sets of ΔV curves display clear trends, with marked differences between the DD and UD differentials, averaging 10–15 cm s^{-1}. The DD drifter 0070 has uninterrupted GPS transmissions and small velocity differences with the drogued neighboring drifters below 5 cm s^{-1} throughout almost all of its life span. The nearby undrogued drifters clearly have higher downwind speeds.

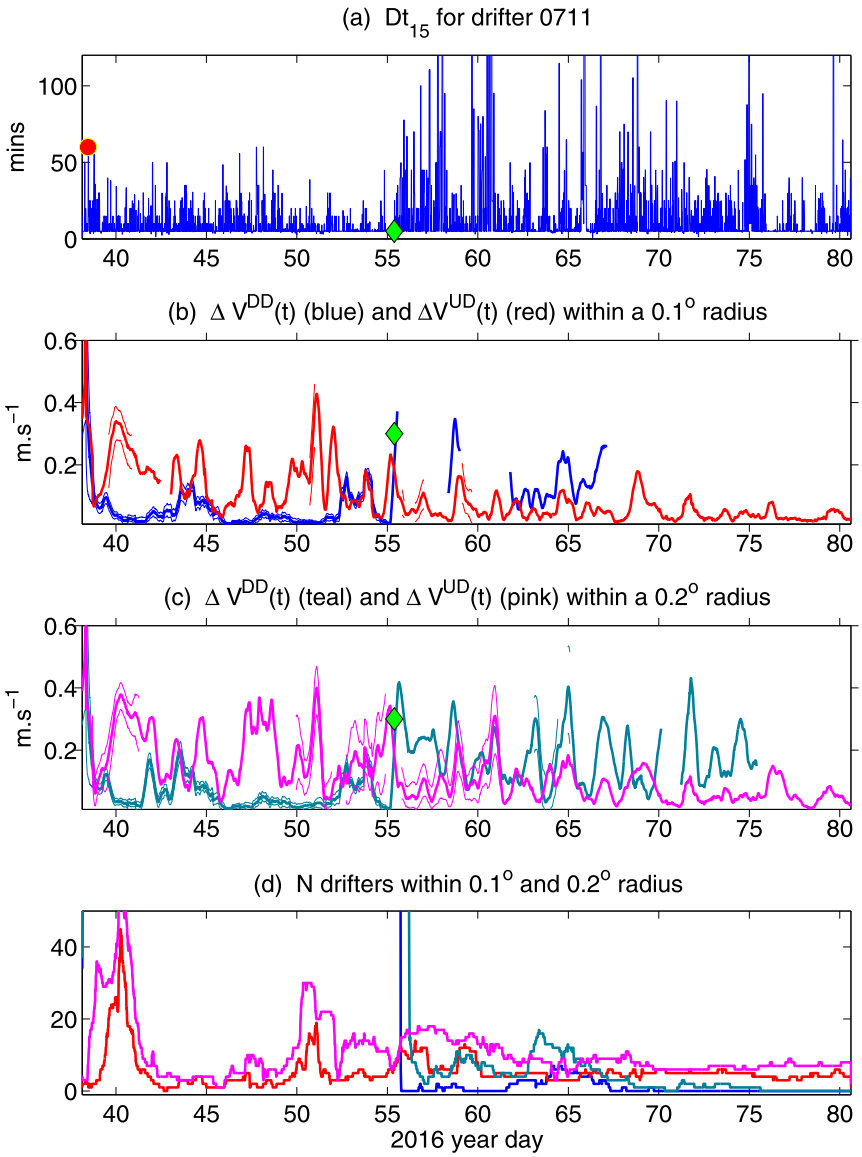

FIG. 10. (a) The DT_{15} of stage 1 UU drifter 0711 from the LDA launch vs time. The earliest time anomalous GPS transmissions suggest drogue loss (red disk) and the drogue-loss time t^L determined during stage 2 (green diamonds). (b) The 10-h low-pass filtered $\Delta V^{\mathrm{DD}}(t)$ (blue line) and $\Delta V^{\mathrm{UD}}(t)$ (red line) from neighboring drifters within a 0.1° radius. The 95% confidence intervals for ≥10 neighbors are also plotted. (c) The $\Delta V^{\mathrm{DD}}(t)$ (teal line) and $\Delta V^{\mathrm{UD}}(t)$ (pink line) from a 0.2° radius neighborhood. (d) The number of drifters (displayed when lower than 50) involved in each computation of the $\Delta V(t)$.

As for the UD drifter 0102, the drogue loss shortly after its release is clearly reflected in both the transmission and the ΔV time series, as it is for many drifters affected by the storm on 22 January. All the drifters show the trend reversal of the ΔV^{DD} and ΔV^{UD} curves seen in the example on yearday 23. In this case, the first estimated time of drogue loss was correct.

Note that for drogue losses happening in dense populations of DD and UD drifters, t^L can be estimated with a precision of less than half an hour via the raw ΔV time series. The number of drifter neighbors generally decreases over time, until it reaches a point where the results are no longer meaningful from a statistical standpoint. For instance, the bootstrapping method used to calculate confidence intervals is not reliable for fewer than 10 drifters. However, even with a single drifter ΔV can be computed and used in conjunction with visual analysis of the Lagrangian animation to determine a likely drogue-loss time.

TABLE 2. Cumulative number of drifters in each category after stage 1, the first iteration of stage 2 (2a), the fourth iteration of stage 2 (2b), and after visual inspection (2c) on 8 Mar 2016.

Stages	DD	UD	UU
Stage 1	382	257	362
Stage 2a	582	327	92
Stage 2b	605	349	47
Stage 2c	595	395	11

There is a certain degree of subjectivity in the qualitative process of visual analysis that is part of the methodology. Nonetheless, the drogue status is generally clear and consistent with the ΔV curves even with low statistical significance.

After another iteration of stage 2 (stage 2b in Table 2), the number of UU drifters was reduced to 47 by 8 March (yearday 68), with 605 DD and 349 UD drifters (stage 2b). The remaining 47 UU drifters can be divided into two categories: a small number with sporadic transmission leading to bad time interpolations and unrealistic velocities, and the rest having been entrained into the GoM interior and being advected by the dominant mesoscale circulation. Their ΔV curves have too many gaps and/or are irregular, without enough distinctions between

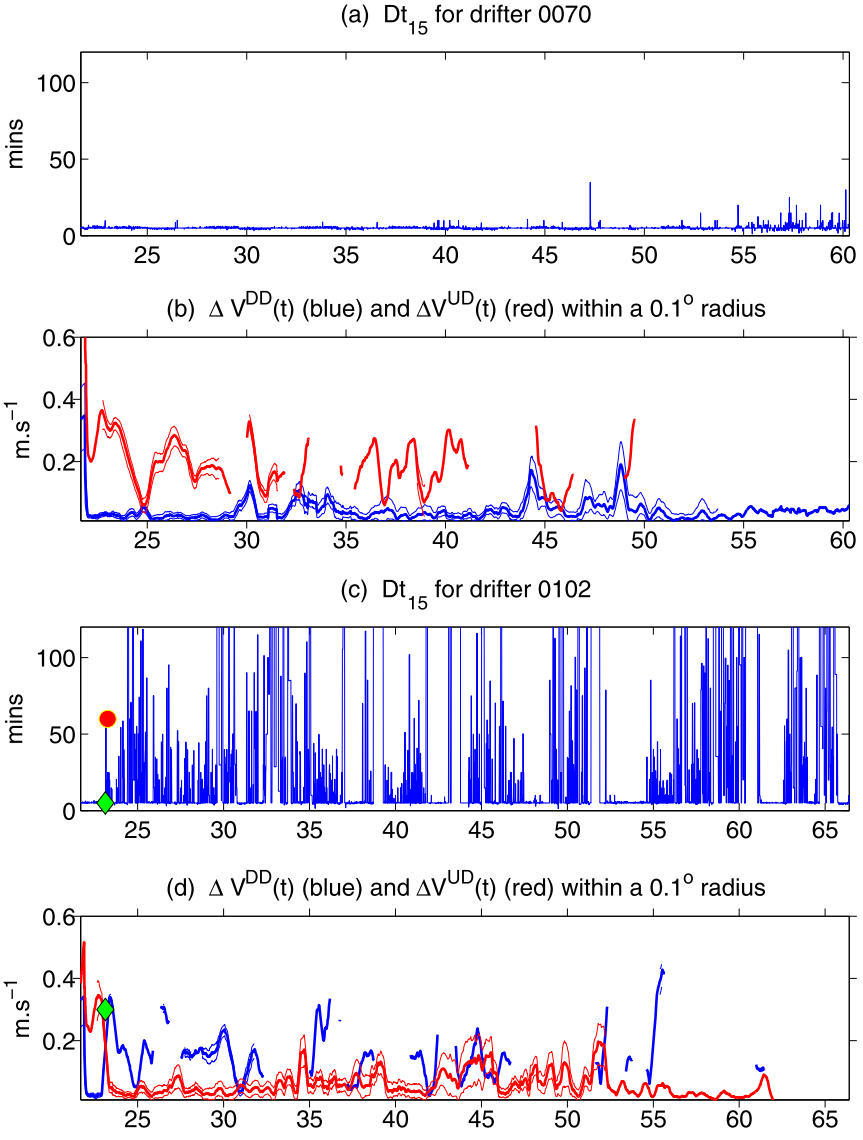

FIG. 11. (a) The DT_{15} of DD P1 drifter 0070 vs time (yearday). The earliest time anomalous GPS transmissions suggest drogue loss (red disk) and the drogue-loss time t^L determined during stage 2 (green diamonds). (b) The 10-h low-pass filtered $\Delta V^{DD}(t)$ (blue line) and $\Delta V^{UD}(t)$ (red line) from neighboring drifters within a 0.1° radius. The 95% confidence intervals for ≥10 neighbors are also plotted. (c),(d) As in (a) and (b), respectively, but for the UD P1 drifter 0102.

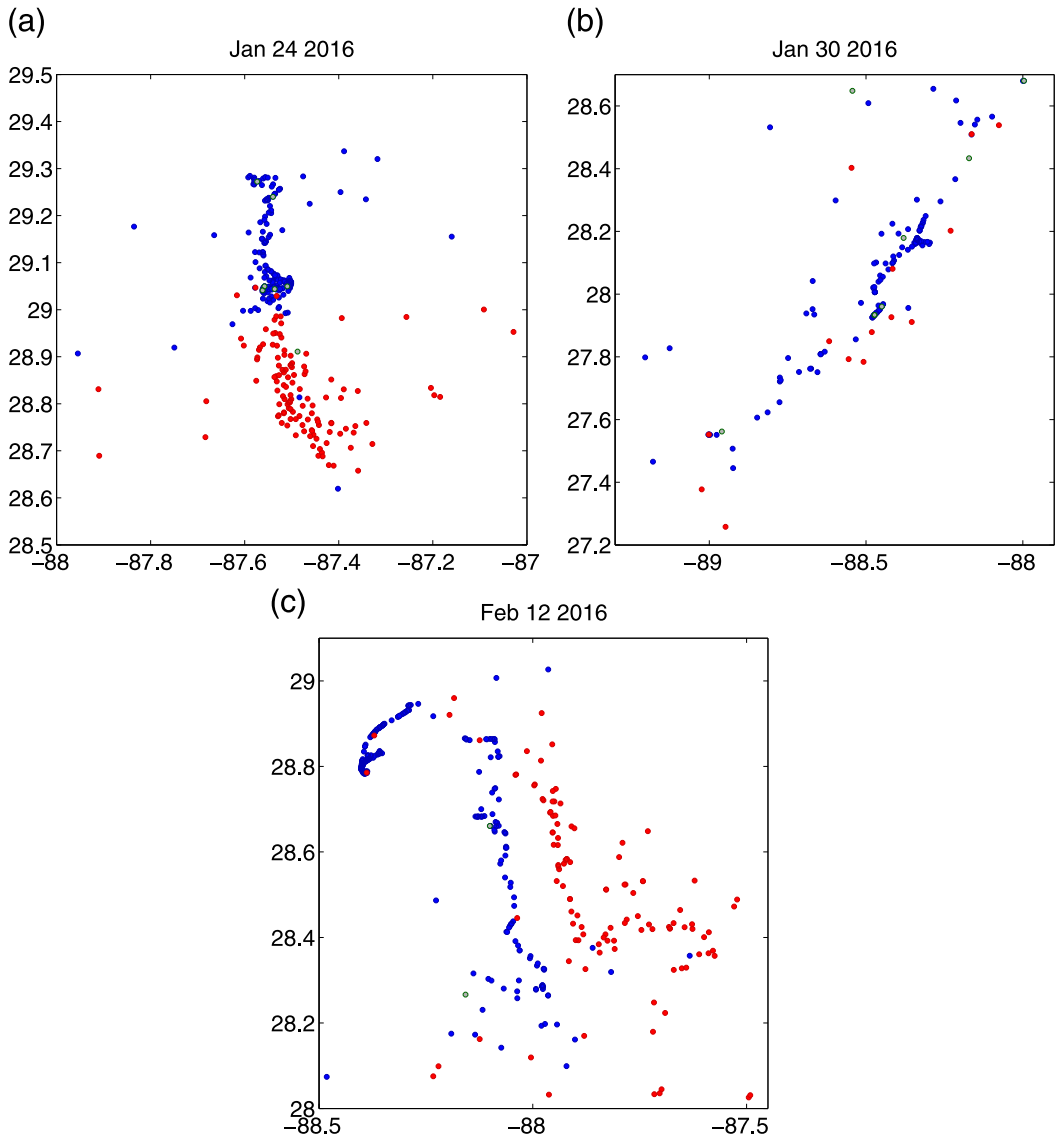

FIG. 12. The drifter distributions at the end of stage 2 for the three main launch groups—(a) P1, (b) P2, and (c) LDA—a few days after their release. The DD (blue), UD (red), and UU (gray) drifters are plotted.

the DD and UD velocities. The UU drifters are still clustered, but they surrounded by other UU drifters.

An additional series of iterations and Lagrangian animations helped classify one drifter at a time and sequentially update the values of ΔV and population distributions, reducing the number of UU drifters to 11, with 595 DD and 395 UD drifters (cf. stage 2c in Table 2). The final classification results are illustrated in Fig. 12; compare that to Fig. 9, which shows the results after stage 1.

The extent to which stage 2 modified the drogue loss times estimated in stage 1 can be assessed by considering the drifters that remained undrogued in both stages, which make about 98% of the UD drifters in stage 1. Out of these, 60% remained the same, 32% were shifted to an earlier date by an average of 0.9 day, and about 6% were shifted to a later time by an average of 2 days.

Regarding the percentage of status change from stage 1 to stage 2, Table 3 summarizes all possible combinations. The UU drifters in stage 1 (36% of the dataset) mostly change from UU to DD (21%) and UU to UD (13%). What would be considered as misdiagnoses in stage 1— that is, changes from DD to UD, UD to DD, DD to UU, and UD to UU—tend to be much lower $\sim O(0–1)\%$. The only reservation would be the changes from 1.6% DD to UD from stage 2b to stage 2c, but these changes are referring to the drifters in the GoM interior needing sequential classification of each drifter (DD and

TABLE 3. Drifter percentages (of the dataset) changing status between consecutive stages.

Stages	UU to DD	UU to UD	DD to UD	UD to DD	DD to UU	UD to UU
1 to 2a	20.5	7.4	0.3	0	0.7	0.2
2a to 2b	2.3	2.2	0	0	0	0
2b to 2c	0.2	3.4	1.6	0	0.2	0
1 to 2c	21	13.1	1.6	0.3	0.2	0

UU) at a time, with extensive use of Lagrangian animations. Overall, these percentages indicate that the final results are very unlikely to be biased by erroneously classifying DD and UD drifters in the first stage.

c. *Extension to 29 March*

Eventually, it became necessary to extend the analysis by a few more weeks to complete the drogue-loss detection for several reasons: First, there was a long wind and wave event spanning 5 days around 8–13 March that coincided with the end of the study period. The number of drogue losses from 8 March was therefore underestimated and required more information from ΔV beyond that time. Second, as the drifter density decreased over time, the drogue status from ΔV became unreliable, and while the Lagrangian animations provided additional feedback, it was necessary to define a range of validity beyond which the drogue state was no longer identifiable. The range of validity was particularly needed for the DD drifters, since there was always the potential of drogue loss while the GPS was still active. Third, a large number of drifters ended up beaching on the shores of Louisiana, Mississippi, and Alabama between 24 February and 20 March. All those recovered later were found to be without drogues. While the drogues could have detached during grounding, it was worth investigating the possibility that a prior wind/wave event might have triggered another series of drogue losses. As the drifters reclustered while they approached the shore, there was again an opportunity to detect their drogue status with the ΔV metric.

Overall, more than 120 drogue losses were detected after 24 February, the date that the first drifters reached the shore. Among them, ≈90 were on the slope and shelf north of 28.5°N. Most of the drifters on or close to the continental shelf belong to the LDA launch. The first major launch (P1) in January suffered heavy drogue losses early, which resulted in early battery depletion (from the inverted GPS struggling to relay the signal to the satellites), leaving only a few active in March, while the P2 drifters were entrained quickly into the GoM interior. The massive drogue losses of 7–9 March on the shelf south of Mobile Bay is an interesting phenomenon, since it was found that sustained winds from the southeast pushed many undrogued drifters to beach while the drogued ones were relatively unaffected. Among the undrogued drifters, a significant number of them lost their drogues shortly before reaching the shore in a small area around (29.2° to 30.1°N, 88.5° to 87°W).

d. *Wave and wind impact*

The estimated times of drogue loss are compared to the mean squared slope, or wave steepness, of the UWIN-CM at the drifter locations. Figure 13a highlights the significant wave events represented by steep wave slopes projected onto the drifter array. Clustered drogue losses can be seen coinciding with the major storm events. The trend is particularly clear shortly after the P1 launch on 21 January (yeardays 21–22), around 9–10 February (yeardays 41–42), 24–25 February (yeardays 55–56), then later on 8–13 March (yeardays 67–72), and on 20–23 March (yeardays 79–82), with the latter two representing mostly the drogue losses occurring near or on the shelf. Note that the last group launch (''test'') contains a number of drifters released undrogued on purpose.

The wind and wave slope distributions for the drogue losses are examined after excluding the drifters from the tests and those whose drogues detached from impact during the launch. The mean squared slope in Fig. 13b depicts at least 50% of the drogue losses occurring with very steep wave slopes (median of 0.03, and maximum occurrences between 0.037 and 0.04), while 20% of the drogue losses occurred with weak slopes ≤ 0.02. On the other hand, Fig. 13c indicates weaker dependence on the strength of the wind. These results merely highlight the already known fact that the surface winds alone do not dictate the wave steepness and confirm that the wave slope is the main factor affecting the drifters' structural integrity by straining the link connecting the tether to the floater. Since the wind events in the GoM trigger the wave events, they are an indirect cause of drogue losses. But the wave events appear to last longer than the wind events, resulting in possible drogue loss shortly before or after the wind event, while the waves are active. For instance, 10 drifters were found to have lost their drogues during light ($<5\,\mathrm{m\,s^{-1}}$) winds and significant wave steepness (>0.025).

Additionally, a few drogue losses occurring during relatively calm seas were found, such as 12 drifters with $<5\,\mathrm{m\,s^{-1}}$ winds and weak mean squared wave slopes < 0.01. These cases show that even during light winds the ΔV metrics find the UD to be ~5–10 $\mathrm{cm\,s^{-1}}$ faster than the DD. We think that the Stokes drift, which amounts to about $5\,\mathrm{cm\,s^{-1}}$ for $5\,\mathrm{m\,s^{-1}}$ winds, can

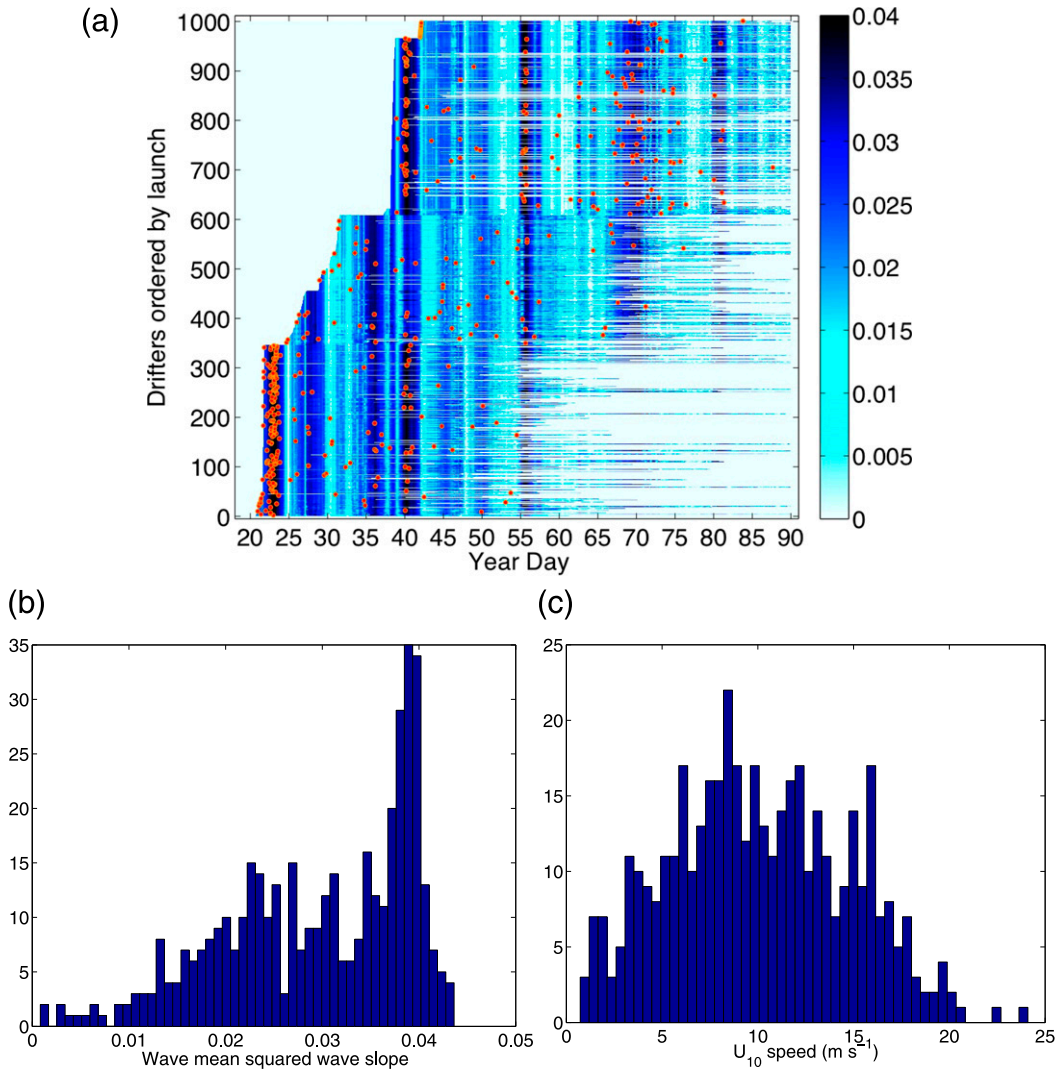

FIG. 13. (a) The mean squared wave slope interpolated to the drifter array, colored by intensity, and times of drogue loss (red dots). The *y* axis corresponds to the drifters reordered by launch dates. (b),(c) Histograms of the wave steepness and 10-m wind speed, respectively, at the locations and times of the drogue losses.

combine with the floater slip, which is more significant during weaker winds (Novelli et al. 2017), to produce a distinct velocity differential even during light wind and wave periods that is well captured by the ΔV metrics with sufficient drifter density. Note that in the unlikely scenario of drogue loss during zero wind and wave, a sustained $\Delta V^{\mathrm{UD}} \approx \Delta V^{\mathrm{DD}}$ should be observed. However, it would be preceded by $\Delta V^{\mathrm{UD}} > \Delta V^{\mathrm{DD}}$ and followed by $\Delta V^{\mathrm{UD}} < \Delta V^{\mathrm{DD}}$, implying a drogue loss occurring during the calm weather period.

e. Uncertainty estimates

Ranges of validity for the drogue state are determined to complete the analysis. They are estimated qualitatively from individual Lagrangian animations. It is possible to detect the drogue status of a drifter at a given time by looking at its spatiotemporal evolution with respect to the surrounding drifters. The upper bound is defined as the time when it becomes visually impossible to distinguish UD behavior from DD behavior. This usually happens when the neighbor population is reduced to 1 or 2, or when the horizontal velocity gradients of the mesoscale flow become dominant. Each animation depicts sharp differences in advection between the two populations that can be summarized as a tendency for DD drifters to align (presumably along fronts) in spite of sustained transverse winds. On the other hand, UD drifters will align only in calm weather and move in a more downwind direction otherwise. During periods of sustained winds and in the presence of

nearby drifters, this discrepancy is very clear and allows the identification of both drogue status and drogue-loss time within hours. Limitations are introduced by the geostrophic circulation of the GoM interior and high wind variability, particularly in direction. For instance, wind fluctuations on the shelf at the end of March prevented the classification of a group of drifters in spite of good drifter density.

Additionally, three levels of precision for the drogue-loss dates are defined upon completion of the drogue-detection analysis. Level 1: A drogue loss occurs during a sustained wind event and in a region of high drifter density. The difference in velocities between drogued and undrogued drifters shows a sharp transition in the raw ΔV trends over one to two data points from the interpolated data, that is, 15–30 min. Level 2: A drogue loss has a longer transition in ΔV, leaving its more accurate detection to the Lagrangian animation. The minimum uncertainty is of the order of the time interval between consecutive snapshots, that is, 3 h. Level 3: The drogue-loss time is unclear from the ΔV curves and the animation, even if the undrogued state is confirmed at later times.

The results for drogue loss and uncertainty times are illustrated in Fig. 14. The highest precision (1/2 h) in t^L is obtained for drifters that were part of the massive drogue losses in the P1 and LDA groups shortly after their releases. It also applied to the major wind events and for the drogue losses near the shore. Together, these amount to 63% of drogue losses by 8 March at level 1 precision. Another 25% of t^L are detected within a 3-h range.

Also displayed in Fig. 14 are the dates and locations of the DD upper bounds. Their spatial distributions tend to be in the GoM interior or at the periphery of the domain covered by the dataset at the beginning of the experiment, while their time distribution indicates weeks beyond launch dates and a preponderance from the P2 launch. It confirms that low drifter density and mesoscale-dominated flows are the main limitations to the drogue detection algorithm.

GPS battery depletion leads to a reduced drifter presence over time (Fig. 15b) versus the cumulative numbers of stage 2c (Fig. 15a). The upper bound on known drogue status contributes to a rapid decrease in the DD population, while the UU numbers increase to $O(100)$ about two weeks after the last release.

f. Validation

The drogue status of some drifters was verified in the field, either as a result of observed drogue detachment upon launch or as observed at later times when the ship passed nearby. Once the drogue issue was identified,

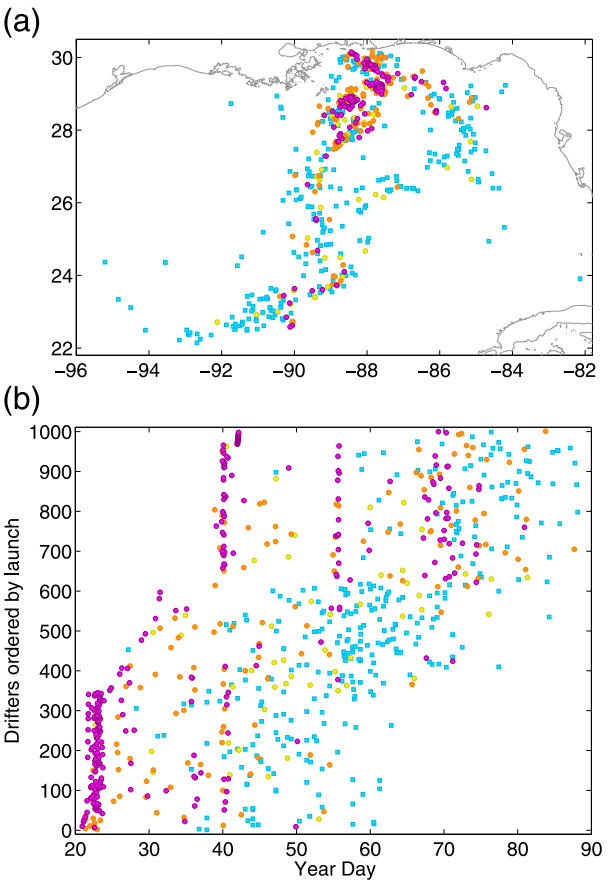

FIG. 14. (a) The locations of drogue loss times t^L with precision levels of 0.5 h (magenta), 3 h (orange), and >3 h (yellow), and locations of DD validity upper bounds (cyan squares). (b) The upper bounds (yearday) of t^L and DD as a function of the drifters reordered by launch dates.

several drifters were also intentionally deployed without drogue alongside drifters with reinforced drogue attachments in the test release to serve as benchmarks. These data points can be used to validate the detection algorithm to a certain extent. Among those observed to have lost their drogues are 13 drifters that broke on impact while thrown from the ships. Their ΔV time series all point to an undrogued status since their launches. There is one exception for drifter 0073, which we think was confused in the log with drifter 0078, which was the immediately next launch: Both ΔV and Lagrangian animations point to the former as drogued and the latter as detached from impact.

The algorithm works similarly well for the 23 drifters launched intentionally without drogues on 10–11 February and for those 5 drifters launched with a strongly attached drogue. Of the nine drifters crossing the paths of the ships at a later time, six were found undrogued, one drogued, and two with damaged drogues. Animations and ΔV time series are found to be consistent with the

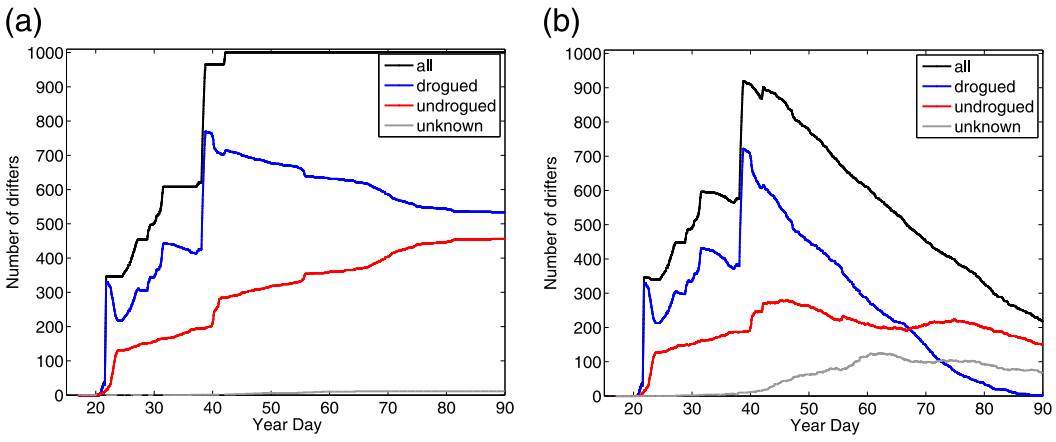

FIG. 15. (a) The cumulative numbers of all (black), DD (blue), UD (red), and UU (gray) drifters as a function of time from the analysis extended to 29 Mar 2016. (b) As in (a), but for the absolute numbers, accounting for drifter loss caused by battery depletion and similar factors.

drogued and undrogued drifters at the time of their encounters. Note that the 23 drogueless drifters from the test launches have corresponding velocity differentials showing from the start a significantly higher ΔV^{DD} than ΔV^{UD} by at least 5–10 cm s^{-1} while their first 10 days were under relatively moderate (3–10 m s^{-1}) winds. These cases indicate that the ΔV metrics do not require major wind events to properly identify the drogue status.

Of the drifters with damaged drogues, one has a signature more suggestive of DD status, while the other behaves more like a UD drifter. So in total, there are 13 + 28 + 9 = 50 drifters serving as ground truth, of which 48 confirm the drogue analysis and 2 technically do not belong to any of the drogue categories because of their damaged drogues. This is a remarkable success rate if we ignore the damaged drogues, which we consider beyond the scope of this study.

5. Summary and discussion

LASER was designed to measure submesoscale near-surface flows in the NGoM in the winter of 2016. The central component was the release of over 1000 mostly biodegradable CARTHE-designed surface drifters, the largest targeted drifter release to date. Most of the drifters were released in three localized clusters, each composed of roughly 300 drifters. The average trajectory lasted about 2 months with a GPS time interval of 5 min. Postprocessing issues included determining accurate launch dates, beaching times, drogue status, and data filtering.

The major challenge addressed in this study is the detection of drogue loss. This is important because drifters with a drogue sample the upper 60 cm, while those without a drogue sample the upper 5 cm and may have significantly greater windage effects. Because of the short time and space scales of this experiment, the existing methods relying on subtraction of the altimetry-based geostrophic velocity field could not be used to isolate the wind contribution. A new method was instead developed by taking advantage of the unique characteristics of LASER. The dense, near-simultaneous launch configurations on the slope led to persistent clustering in regions of relatively weak geostrophic flows and were subjected to frequent periods of strong wind. Drogue loss mostly occurred during these wind events. A significant fraction of the dataset in the following weeks could then be easily classified as drogued or undrogued, because the undrogued drifters were prone to transmission problems and tended to move faster during the wind events and because the drogued drifters tended to align along convergence zones between wind events.

The drogue detection algorithm was composed of two stages: In the first stage, drogued and undrogued populations were established from a first guess based on the combination of two criteria: the rate of GPS transmission and the average downwind velocity. Relatively fast downwind velocities and anomalously low GPS transmission rates are the signature of an undrogued drifter. The drogue status of about 60% of the LASER drifters was established in this way. In the second stage, the velocities of the remaining drifters were compared to those of nearby drifters of known status. This was done both quantitatively via velocity metrics and visually via animations of the drifter motions. The process was iterative with the newly identified drifters adding to the known populations and allowing the status of additional drifters to be determined. This was continued until convergence to a final result. The time series of the

velocity differentials between a drifter of unknown drogue status and known drogued and undrogued groups leave a clear signature of the drogue loss and thus an accurate estimate of the time of drogue loss. When the drogue loss occurs in a region of high drifter density, the date can be determined to within half an hour.

Fifty drifters, which either broke their drogues off from impact during their releases, were launched intentionally without drogues, or were intersected at a later time by the ships, served as a control to evaluate the performance of the algorithm. It was found that the drogue status of virtually all of them is consistent with the results, excepting those with damaged drogues and a suspected deployment log error. The accuracy of the proposed algorithm for this subset of drifters was thus 94%–100%.

Ranges of validity are estimated for each drifter without identified drogue-loss time. These are better alternatives to confidence intervals for the DD population, which can become low relatively quickly when the drifter density starts to decrease. The individual Lagrangian animations can prolong the confidence in the estimate, albeit qualitatively only. After the LDA launch, the number of known drogued drifters decreases fast over time, as batteries are depleted and the drifters disperse in the GoM interior.

By the first week of March (i.e., 50 days after the start of the experiment), about 40% of the drifters lost their drogues, the majority of them during storm events accompanied by steep waves. Close to 90% of drogue-loss times are estimated with a precision of a few hours, including 60% within a half hour. The DD numbers present in the GoM decrease from 162 out of 468 on 8 March down to 1 out of 228 on 29 March. A second significant drogue-loss period was identified among groups of drifters on the shelf approaching the shoreline. The clustering distribution helped estimate the times of loss and confirmed that most of the beached drifters were indeed without drogues.

An interesting consequence of the unintended drogue losses is that the two distinct drifter populations illustrate the major differences in flow dynamics between the first few centimeters and the upper one-half meter. Since both circulations are particularly relevant to dispersion of pollutants, the vast drifter dataset of LASER is contributing doubly to a better understanding of surface and interface dynamics. Furthermore, the many instances when drifter clusters of both DD and UD intersect provide valuable information on the vertical shear in the upper-half meter, the surface wind, and the Stokes drift—all of which can help in Lagrangian parameterization and prediction.

While it was tailored for LASER, this method for drogue-loss detection may be applied to large releases of dense drifter clusters in coastal waters where mesoscale motions are mostly absent. Indeed, the main requirements of this method are a sustained high drifter density and a surface circulation with little or no mesoscale motions. In a scenario where the drogue loss times are more randomly distributed, the metrics of stage 1 can be combined from the beginning by using the estimated times of loss from Q to remove the still-drogued trajectory portions. The surface winds need not be extreme: unless the wind is absent, there is always enough momentum from the Stokes drift and the floater's slip to deduce the drogue status from the time series of the velocity differentials. In light of the recent advances in Lagrangian oceanography where the focus has shifted toward coastal small-scale flows, massive drifter releases within small areas will probably become common in the near future, and this method could be useful beyond LASER.

Acknowledgments. The authors wish to recognize the tremendous effort that was needed for planning and executing LASER, which involved many people but too many to list here. This research was made possible by a grant from the Gulf of Mexico Research Initiative (Grant SA-1515 CARTHE). Raw, processed drifter trajectory data, and drogue classification results are publicly available through the Gulf of Mexico Research Initiative Information and Data Cooperative (GRIIDC; https://data.gulfresearchinitiative.org; https://doi.org/10.7266/N7MS3R6V, https://doi.org/10.7266/N7W0940J, and https://doi.org/10.7266/N7QN656H, respectively). The UWIN-CM data can also be obtained from GRIIDC under https://doi.org/10.7266/N7KW5DH7. The authors thank the three anonymous reviewers, who helped greatly improve the manuscript.

REFERENCES

Berta, M., A. Griffa, M. G. Magaldi, T. M. Özgökmen, A. C. Poje, A. C. Haza, and M. J. Olascoaga, 2015: Improved surface velocity and trajectory estimates in the Gulf of Mexico from blended satellite altimetry and drifter data. *J. Atmos. Oceanic Technol.*, **32**, 1880–1901, https://doi.org/10.1175/JTECH-D-14-00226.1.

Chen, S. S., and M. Curcic, 2016: Ocean surface waves in Hurricane Ike (2008) and Superstorm Sandy (2012): Coupled modeling and observations. *Ocean Modell.*, **103**, 161–176, https://doi.org/10.1016/j.ocemod.2015.08.005.

——, W. Zhao, M. A. Donelan, and H. L. Tolman, 2013: Directional wind–wave coupling in fully coupled atmosphere–wave–ocean models: Results from CBLAST-Hurricane. *J. Atmos. Sci.*, **70**, 3198–3215, https://doi.org/10.1175/JAS-D-12-0157.1.

Curcic, M., S. S. Chen, and T. M. Özgökmen, 2016: Hurricane-induced ocean waves and Stokes drift and their impacts on surface transport and dispersion in the Gulf of Mexico. *Geophys. Res. Lett.*, **43**, 2773–2781, https://doi.org/10.1002/2015GL067619.

D'Asaro, E. A., and Coauthors, 2018: Ocean convergence and the dispersion of flotsam. *Proc. Natl. Acad. Sci. USA*, **115**, 1162–1167, https://doi.org/10.1073/pnas.1718453115.

Donelan, M. A., M. Curcic, S. S. Chen, and A. K. Magnusson, 2012: Modeling waves and wind stress. *J. Geophys. Res.*, **117**, C00J23, https://doi.org/10.1029/2011JC007787.

Haza, A. C., T. M. Özgökmen, and P. Hogan, 2016: Impact of submesoscales on surface material distribution in a Gulf of Mexico mesoscale eddy. *Ocean Modell.*, **107**, 28–47, https://doi.org/10.1016/j.ocemod.2016.10.002.

Hill, C., C. DeLuca, V. Balaji, M. Suarez, and A. da Silva, 2004: The architecture of the Earth System Modeling Framework. *Comput. Sci. Eng.*, **6**, 18–28, https://doi.org/10.1109/MCISE.2004.1255817.

Huntley, H. S., B. L. Lipphardt Jr., G. A. Jacobs, and A. D. Kirwan Jr., 2015: Clusters, deformation, and dilation: Diagnostics for material accumulation regions. *J. Geophys. Res. Oceans*, **120**, 6622–6636, https://doi.org/10.1002/2015JC011036.

Judt, F., S. S. Chen, and M. Curcic, 2016: Atmospheric forcing of the upper ocean transport in the Gulf of Mexico: From seasonal to diurnal scales. *J. Geophys. Res. Oceans*, **121**, 4416–4433, https://doi.org/10.1002/2015JC011555.

Lumpkin, R., S. A. Grodsky, L. Centurioni, M.-H. Rio, J. A. Carton, and D. Lee, 2013: Removing spurious low-frequency variability in drifter velocities. *J. Atmos. Oceanic Technol.*, **30**, 353–360, https://doi.org/10.1175/JTECH-D-12-00139.1.

——, T. M. Özgökmen, and L. Centurioni, 2017: Advances in the application of surface drifters. *Annu. Rev. Mar. Sci.*, **9**, 59–81, https://doi.org/10.1146/annurev-marine-010816-060641.

McWilliams, J., 2016: Submesoscale currents in the ocean. *Proc. Roy. Soc. London*, **472A**, 20160117, https://doi.org/10.1098/rspa.2016.0117.

Mensa, J. A., Z. Garraffo, A. Griffa, T. M. Özgökmen, A. C. Haza, and M. Veneziani, 2013: Seasonality of the submesoscale dynamics in the Gulf Stream region. *Ocean Dyn.*, **63**, 923–941, https://doi.org/10.1007/s10236-013-0633-1.

Niiler, P. P., A. Sybrandy, K. Bi, P. Poulain, and D. Bitterman, 1995: Measurements of the water-following capability of holey-sock and TRISTAR drifters. *Deep-Sea Res. I*, **42**, 1951–1964, https://doi.org/10.1016/0967-0637(95)00076-3.

Novelli, G., C. M. Guigand, C. Cousin, E. H. Ryan, N. J. M. Laxague, H. Dai, B. K. Haus, and T. M. Özgökmen, 2017: A biodegradable surface drifter for ocean sampling on a massive scale: Design, calibration and application. *J. Atmos. Oceanic Technol.*, **34**, 2509–2532, https://doi.org/10.1175/JTECH-D-17-0055.1.

Olascoaga, M. J., and Coauthors, 2013: Drifter motion in the Gulf of Mexico constrained by altimetric Lagrangian coherent structures. *Geophys. Res. Lett.*, **40**, 6171–6175, https://doi.org/10.1002/2013GL058624.

Pazan, S. E., and P. P. Niiler, 2001: Recovery of near-surface velocity from undrogued drifters. *J. Atmos. Oceanic Technol.*, **18**, 476–488, https://doi.org/10.1175/1520-0426(2001)018<0476:RONSVF>2.0.CO;2.

Phillips, O. M., 1977: *Dynamics of the Upper Ocean.* Cambridge University Press, 336 pp.

Poje, A. C., and Coauthors, 2014: Submesoscale dispersion in the vicinity of the *Deepwater Horizon* spill. *Proc. Natl. Acad. Sci. USA*, **111**, 12 693–12 698, https://doi.org/10.1073/pnas.1402452111.

Poulain, P. M., R. Gerin, and E. Mauri, 2009: Wind effects on drogued and undrogued drifters in the eastern Mediterranean. *J. Atmos. Oceanic Technol.*, **26**, 1144–1156, https://doi.org/10.1175/2008JTECHO618.1.

Rio, M.-H., 2012: Use of altimeter and wind data to detect the anomalous loss of SVP-type drifters drogue. *J. Atmos. Oceanic Technol.*, **29**, 1663–1674, https://doi.org/10.1175/JTECH-D-12-00008.1.

Skamarock, W. C., and Coauthors, 2008: A description of the Advanced Research WRF version 3. NCAR Tech. Note NCAR/TN-475+STR, 113 pp., http://dx.doi.org/10.5065/D68S4MVH.

Stokes, G. G., 1847: On the theory of oscillatory waves. *Trans. Cambridge Philos. Soc.*, **8**, 441–455.

Wallcraft, A. J., E. J. Metzger, and S. N. Carroll, 2009: Software design description for the HYbrid Coordinate Ocean Model (HYCOM) version 2.2. NRL Memo. Rep. NRL/MR/7320–09-9166, 155 pp.

Yaremchuk, M., and E. F. Coelho, 2015: Filtering drifter trajectories sampled at submesoscale resolution. *IEEE J. Oceanic Eng.*, **40**, 497–505, https://doi.org/10.1109/JOE.2014.2353472.

Zhong, Y., A. Bracco, and T. A. Villareal, 2012: Pattern formation at the ocean surface: *Sargassum* distribution and the role of the eddy field. *Limnol. Oceanogr. Fluids Environ.*, **2**, 12–27, https://doi.org/10.1215/21573689-1573372.

Zhu, P., Y. Wang, S. S. Chen, M. Curcic, and C. Gao, 2016: Impact of storm-induced cooling of sea surface temperature on large turbulent eddies and vertical turbulent transport in the atmospheric boundary layer of Hurricane Isaac. *J. Geophys. Res. Oceans*, **121**, 861–876, https://doi.org/10.1002/2015JC011320.